Effect of Sensitizer Adsorption Temperature on the Performance of Dye-Sensitized Solar Cells

ARTICLE *in* JOURNAL OF THE AMERICAN CHEMICAL SOCIETY · JUNE 2011

Impact Factor: 12.11 · DOI: 10.1021/ja110541t · Source: PubMed

JACS
JOURNAL OF THE AMERICAN CHEMICAL SOCIETY

ARTICLE

pubs.acs.org/JACS

Effect of Sensitizer Adsorption Temperature on the Performance of Dye-Sensitized Solar Cells

Frédéric Sauvage,*[,†] Jean-David Decoppet,[†] Min Zhang,[†,‡] Shaik Mohammed Zakeeruddin,[†] Pascal Comte,[†] Mohammad Nazeeruddin,[†] Peng Wang,[†,‡] and Michael Grätzel*[,†]

[†]Laboratoire de Photonique et Interfaces, Institut des Sciences et Ingénieurie Chimiques, Ecole Polytechnique Fédérale de Lausanne (EPFL), Station 6, CH-1015 Lausanne, Switzerland

[‡]State Key Laboratory of Polymer Physics and Chemistry, Changchun Institute of Applied Chemistry, Chinese Academy of Sciences, 130022 Changchun, China

Supporting Information

ABSTRACT: Employing a mesoscopic titania photoanode whose bilayer structure was judiciously selected to fit the optoelectronic characteristics of the Ru-based heteroleptic complex Na−*cis*-Ru(4,4′-(5-hexyltiophen-2-yl)-2,2′-bipyridine)(4-carboxylic-acid-4′-carboxylate-2,2′-bipyridine)(thiocyanate)$_2$, coded as C101, we investigated the effect of temperature for dye adsorption on the photovoltaic performance of dye-sensitized solar cells (DSCs). We found a significant efficiency enhancement upon lowering the temperature applied during the sensitizer uptake from solution. When the dye adsorption was performed at 4 °C, the photovoltaic performance parameters measured under standard reporting conditions (AM1.5 G sunlight at 1000 W/m^2 intensity and 25 °C), i.e., the open circuit voltage (V_{oc}), the short circuit photocurrent density (J_{sc}), the fill factor (FF), and consequently the power conversion efficiency (PCE), improved in comparison to cells stained at 20 and 60 °C. Results from electrochemical impedance spectroscopy (EIS) and attenuated total reflection Fourier-transform infrared spectroscopy (ATR-FTIR) show that the self-assembled layer of C101 formed at lower temperature impairs the back-electron transfer from the TiO_2 conduction band to the triiodide ions in the electrolyte more strongly than the film produced at 60 °C. Profiting from the favorable influence that the low-temperature dye uptake exerts on photovoltaic performance, we have realized DSCs showing a power conversion efficiency of 11.5%.

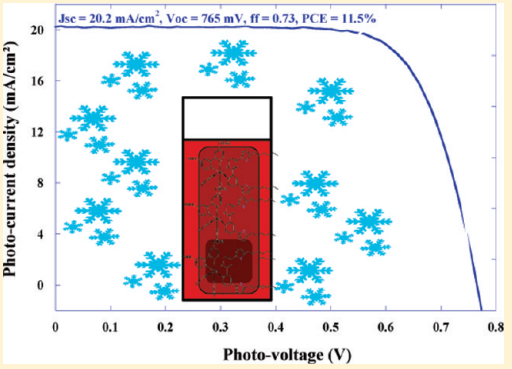

INTRODUCTION

Dye-sensitized solar cells (DSCs) are the only photovoltaic devices that achieve the separation of light absorption from the charge carrier transport (TiO_2) in a photoelectric conversion process. They also are the only truly molecular photovoltaic cells, as the sensitizer molecules harvest sunlight and generate charge carriers, mimicking the light reaction of natural photosynthesis. The DSC has been receiving increasing attention since the demonstration of 7.9% conversion efficiency back in 1991 and is presently studied on a worldwide scale.[1] The recent advancements in the certified conversion efficiency to levels of 11.1% for laboratory cells[2] and 10% for modules[3] provide a mark of maturity and viability of the DSC.

Presently research efforts continue in order to fill the gap between today's benchmark and the Shockley−Queiser limit of $\eta = 32\%$ predicted for a single junction DSC exposed to standard air mass (AM) 1.5 global sunlight (1000 W/m^2 intensity) and capturing all photons below the optimal threshold wavelength of about 920 nm.[4] All possible avenues capable of enhancing the open circuit voltage (V_{oc}), short circuit photocurrent density (J_{sc}), and fill factor (FF) require careful scrutiny and in particular those which promise to improve further the most efficient cells achieving power conversion efficiencies (PCEs) over 10%. Among the successful approaches are enhancements of the lifetime of photogenerated charge carriers and increased panchromatic absorption. Methods applied to prolong the electron lifetimes consist of a conformal coating of the mesoscopic titania film by a 1−2 nm thick oxide overlayer that possesses a higher conduction band than TiO_2 (e.g., ZrO_2, Al_2O_3)[5−7] or by using organic molecular insulators as coadsorbents along with the dye solution or electrolyte.[8−11] This impedes the recapture of the photoinjected electrons by the triiodide in the electrolyte. Coadsorbents added to the dye solution, such as chenodeoxycholic acid (CDCA), prevent also the formation of dye aggregates, which is beneficial for the performance of the cells promoting the kinetics of electron injection and/or dye regeneration.[9] Beside a complementary set of approaches that have also shown promise, e.g., the utilization of the rutile-type polymorph as scattering layer[12] or incorporation of photonic

Received: November 30, 2010

   dx.doi.org/10.1021/ja110541t | J. Am. Chem. Soc. XXXX, XXX, 000–000

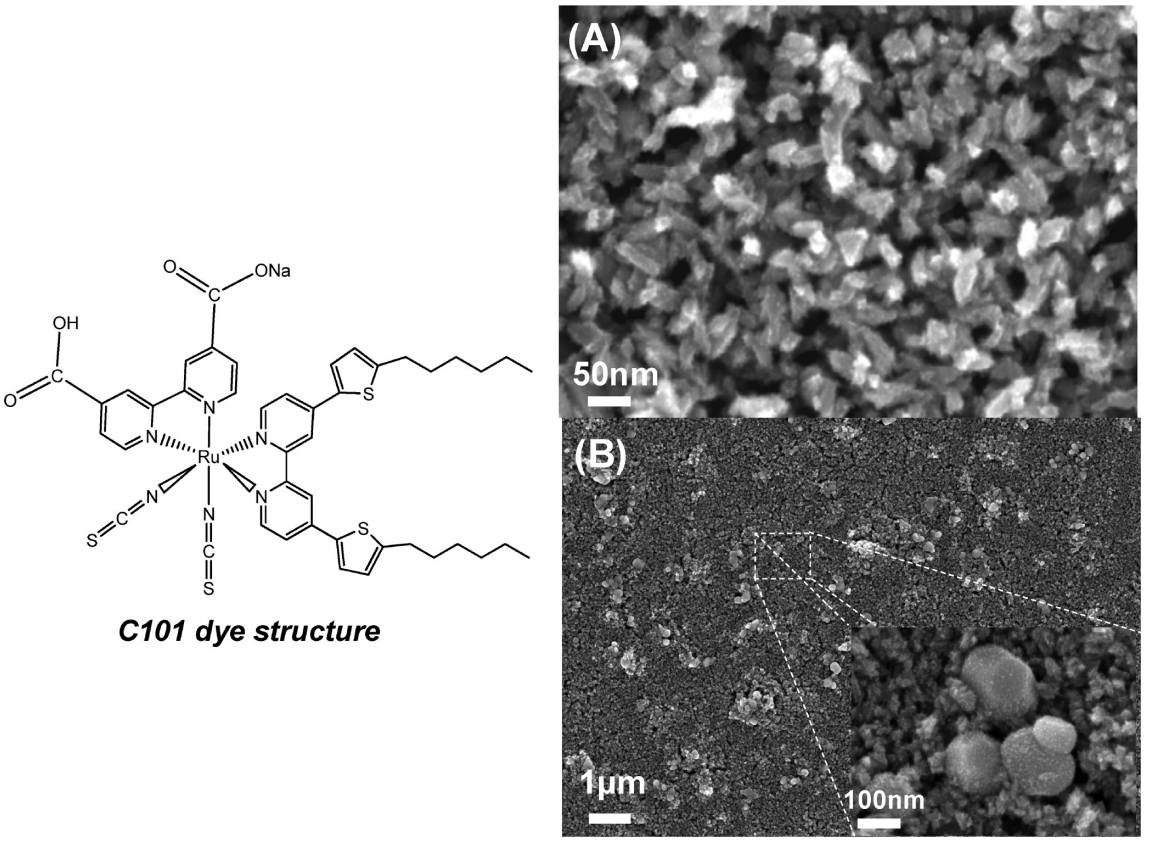

Figure 1. Scanning electron microscope micrographs of (a) the 8.5 μm thick transparent layer and (b) the 6.5 μm opaque layer used as a light reflector. Included is the structure of the C101 complex.

bandgap crystals.[13,14] A remarkable step forward was recently achieved by the design of a new class of heteroleptic Ru complexes whose optical cross-section is significantly enhanced due to the presence of π-conjugated thiophene ligands. This novel series of sensitizers, coded CYC-B or SJW-E[15−17] and the C-100 series,[18−20] exhibit higher molar extinction coefficients as well as lower energy metal-to-ligand charge-transfer (MLCT) bands displaying improved red absorbance as compared to the standard Ru-based complex. Preliminary reports of their photovoltaic characteristics highlight competitive performances as compared to the actual benchmark sensitizers and therefore pave the way to achieve new record efficiencies for the DSC. Here we reveal a beneficial effect of lowering the temperature during the adsorption process of the sensitizer monolayer at the mesoscopic titania surface. The results provide important new insight into the effect of the structure and self-organization of the sensitizer monolayer on the photovoltaic performance of the DSC. So far, there have been surprisingly few investigations, where the dye adsorption temperature was varied in a systematic fashion to check its effect on the solar cell output. Adsorption temperatures above 25 °C have been occasionally applied to accelerate the rate of dye uptake from the solution. However, to the best of our knowledge, none of the previous work has attempted to examine the behavior of a DSC whose sensitizer was adsorbed below room temperature.

RESULTS AND DISCUSSION

Photovoltaic experiments employed the new sensitizer, Na−Ru(4,1′-bis(5-hexylthiophen-2-yl)-2,2′-bipyridine)(4-carboxylic acid-4′-carboxylate-2,2′-bipyridine)(thiocyanate)$_2$ (coded as C101), synthesized according to ref 18. Figure 1 shows the chemical structure of the C101 complex, which resembles that of the amphiphilic Z907Na dye except that thiophene groups are inserted between the 2,2′-bipyridine ligand and the two alkyl chains. Note also the close relationship with the so-called CYC-B3 dye, the latter employing bis-thiophene and longer alkyl chain (C_8H_{17}) substituents on the bpy (bipyridine) ligand.[16] The incorporation of the electron-rich thiophene groups shifts the lowest energy band of the UV−vis absorption spectrum of the C101 to 547 nm as compared to 525 nm for Z907Na and causes an increase in the molar extinction coefficient (ε) from $\varepsilon = 12.2 \times 10^{3}$ [21] to 17.5×10^{3} $M^{-1}\cdot cm^{-1}$.[18] The 22 nm red shift originates from the increased donor strength of the ancillary ligand due to the extension of π-conjugation, destabilizing the metal t_{2g} orbitals.

Before checking the effect of dye adsorption temperature on the device performance, the TiO_2 double layer film morphology was adapted to match the optical properties of the C101 dye in order to yield solar cells with the highest possible power output. The size and shape of the anatase TiO_2 particles constituting the transparent and the scattering layer were varied to ascertain the highest incident photon-to-electron conversion efficiency (IPCE) extending light harvesting furthest into the red and near-IR wavelength region. For reasons of conciseness, the optical characteristics of the different electrode designs as well as their impact on the C101 performance are not detailed here but will be reported elsewhere. The best conversion efficiency was obtained by associating a transparent 8.5 μm thick layer of TiO_2 particles,

dx.doi.org/10.1021/ja110541t |J. Am. Chem. Soc. XXXX, XXX, 000–000

produced by alkaline precipitation of amorphous titania, with a 6.5 μm thick screen-printed overlayer made from Dyesol "active opaque" paste (DSL 18NR-AO) that contains larger light reflecting titania particles. Most of the improvement results from the use of the 18NR-AO paste that is composed of a mixture of slightly elongated rods of ca. 16 × 52 nm in size and scattering 200 nm particles as deduced by scanning eleectron microscopy (SEM). Although the introduction of small particles reduces slightly the reflectance of the scattering layer, this is adequately compensated for by a significant reduction of light loss due to normal deflection by the CCIC−400 nm scattering particles and a larger capacity for dye uptake by the active opaque film.

The SEM micrographs of the transparent and opaque layer are shown in Figure 1. The former is constituted of 23 × 69 nm sized rodlike particles, N_2 sorption experiments showing a type IV isotherm characteristic for the presence of mesopores. Following $TiCl_4$ treatment and sintering, the Brunauer−Emmett−Teller (BET) surface area of those rods was 61 m^2/g, while the porosity of the film was 59%. The association of the two layers still ensures a high BET surface area of ca. 51 m^2/g, thus maintaining a high capacity for dye uptake. The porosity of the film attained 52% after $TiCl_4$ treatment and sintering, corresponding to an average pore diameter of around 25 nm. These structural features are appropriate to support the transport of iodide and triiodide during photovoltaic operation of the cell at full sun, while providing sufficient connectivity between the titania particles to afford efficient electron percolation across the nanocrystalline film to the front contact.

These double layer films were subsequently employed to evaluate the influence of the C101 grafting temperature on the photovoltaic properties. Table 1 shows the device characteristics, i.e., V_{oc}, J_{sc}, FF, and PCE under standard AM 1.5 sunlight and for different temperatures of sensitization. Note that the values reported in this table represent an average for measurements conducted on different cells. Further details relative to the separate values recorded either on square-type electrodes or on masked spots are reported as Supporting Information (Tables S1 and S2). The V_{oc} values obtained were 715, 752, and 766 mV for adsorption temperatures of 60, 20, and 4 °C, respectively. This remarkable increase is accompanied by an improvement in the values of the FF from 0.704 to 0.724, the J_{sc} from 20.7 to 20.8 mA/cm^2, and the PCE from 10.5 to 11.5%. Figure 2 presents a typical ($J-V$) curve recorded on a low-temperature sensitized C101 cell under different light intensities. A similar trend was also observed at lower incident light intensity than 100 mW/cm^2, an efficiency of 11.7% being reached at half sun intensity, i.e., 50.8 mW/cm^2 (V_{oc} = 747 mV, J_{sc} = 11.5 mA/cm^2, and FF = 0.76). Attempts to lower the dye adsorption temperature further to −20 °C were unsuccessful due to low solubility of C101 at this temperature (in ethanol).

Figure 2 also shows the dark current as a function of the potential for the three different dye adsorption temperatures, the current−voltage measurements being carried out at room temperature. The curves highlight a shift toward increased forward bias voltage when the adsorption temperature is decreased. This originates from the higher overpotential for the electrochemical reduction of I_3^- by conduction band electrons at the dye-loaded TiO_2 surface. Apparently the monolayer formed at 4 °C impairs

Table 1. Evolution of the Cells Characteristics as a Function of the Temperature of Sensitization with C101 Dye[a]

	for given temperature of sensitization		
	4 °C	20 °C	60 °C
V_{oc} (mV)	766	752	715
J_{sc} (mA/cm^2)	20.8	20.6	20.7
FF	0.724	0.707	0.704
η (%)	11.5	11.1	10.6

[a] Note that the values tabulated represent an average. The dispersion in the values is reported as Supporting Information.

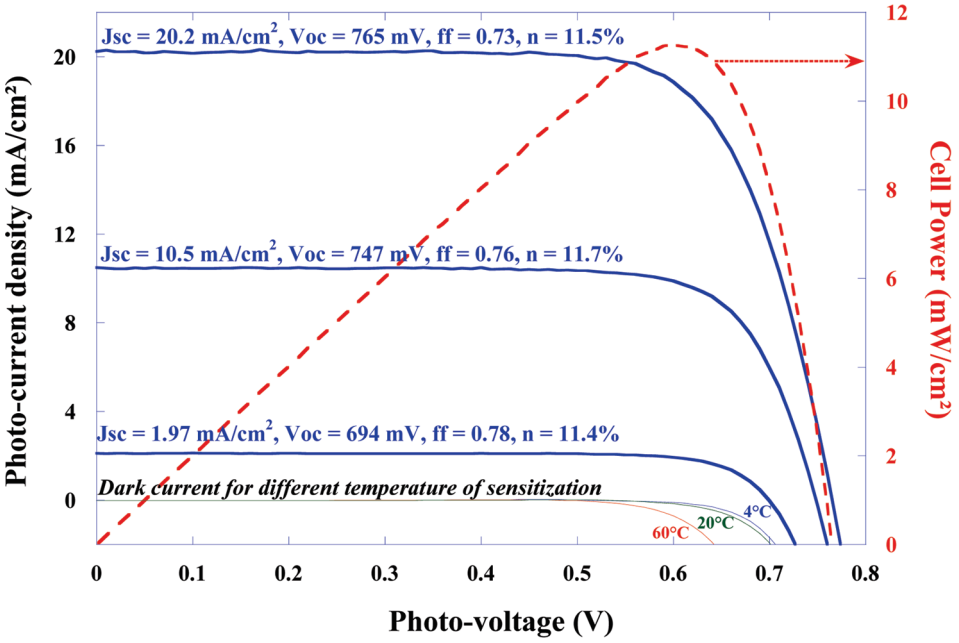

Figure 2. $J-V$ characteristics of C101 dye grafted at 4 °C during 16 h at 1 sun, 0.5 sun, 0.1 sun superimposed to voltamperograms recorded in the dark at a scan rate of 50 mV/s for cells sensitized at 60, 20, and 4 °C (the measurements were conducted at room temperature).

dx.doi.org/10.1021/ja110541t |J. Am. Chem. Soc. XXXX, XXX, 000–000

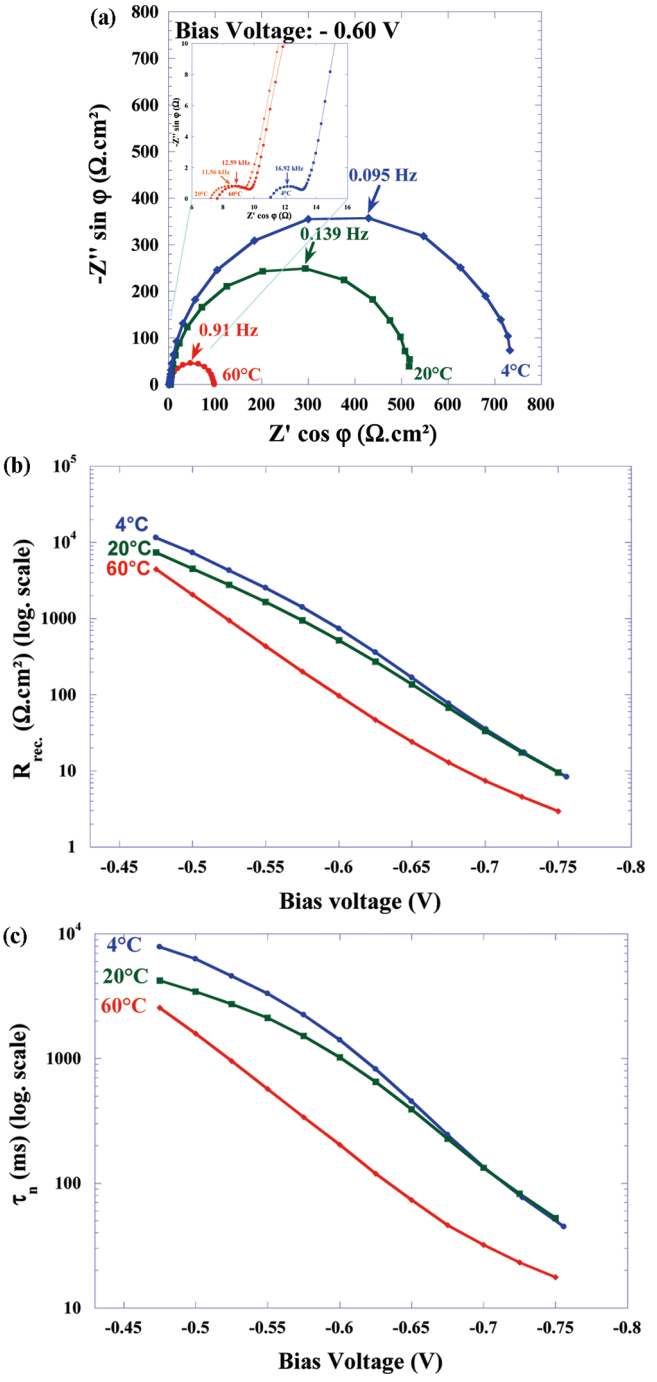

Figure 3. (a) Electrochemical impedance spectra on mesoporous TiO_2 electrode sensitized with the C101 dye at 60, 20, and 4 °C under dark condition with −0.60 V bias voltage, (b) dependnce of the logarithm of R_{rec}, and (c) electron lifetime on the applied bias voltage.

this unwanted dark current more strongly than the one formed at 60 °C. Clearly, the self-assembled sensitizer monolayer is configured differently depending on the adsorption temperature. This state is memorized when the film is incorporated in a fully functional device with measurements made at 25 °C at least for a week. A similar evolution has been observed for cells sensitized either from a solution containing the cheno-deoxycholic acid with a molar ratio of 1/1 or free of the coadsorbant, although the efficiencies in these cases were about 0.2% lower. This confirms

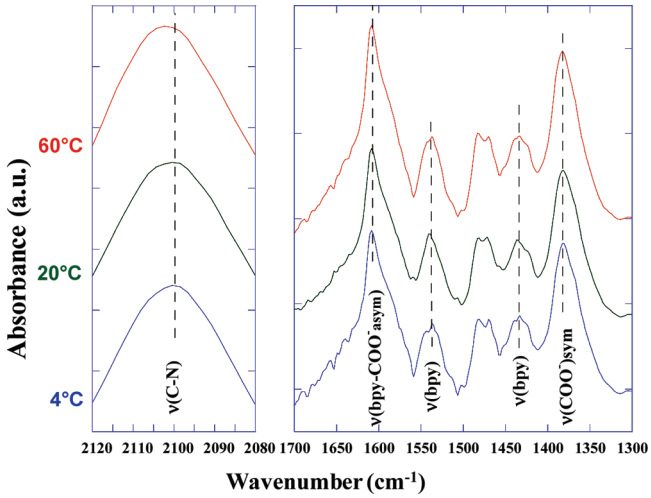

Figure 4. ATR-FTIR spectra of TiO_2 nanocrystalline film loaded with the C101 sensitizer at 4, 20, and 60 °C.

that the coadsorbant does not play a noticeable role in this behavior.

Electrochemical impedance spectroscopy (EIS) was employed to scrutinize the effect of adsorption temperature on the rate of interfacial redox processes. The Nyquist plot of a liquid electrolyte DSC cell generally presents three semicircles. The high-frequency arc, which displays a relaxation frequency of about 10−20 kHz, reflects the reduction of triiodide to iodide at the Pt-loaded TCO counter electrode. The second larger semicircle in the millihertz frequency domain reflects a Nernst or Gerischer-type impedance, showing simultaneously the electrons' diffusion across the nanocrystalline titania layer and their recapture by triiodide at the sensitized-TiO_2/electrolyte interface.[22,23] The third lower frequency arc reveals the triiodide mass transport within the electrolyte governed by a finite-Warburg impedance. This is discernible only in higher viscosity electrolytes such as solvent-free ionic liquids. The simulation of the DSC response uses an equivalent circuit that depicts a general transmission line derived from the well-established macroscopic homogeneous porous electrode model.[24]

Impedance spectra were recorded over the 100 kHz to 10 mHz frequency range in the dark between −0.475 and −0.75 V bias voltage. Nyquist plots for the three temperatures are shown in Figure 3a. The small arc located in the 10−20 kHz range reflects the very low charge-transfer resistance at the counter electrode (R_{ct} = 0.8 Ω·cm^2) achieved by using our acetonitrile-based electrolyte composition. Decreasing the dye adsorption temperature has no effect on the latter feature but augments significantly the diameter of the medium frequency semicircle, reflecting an increase of the resistance for interfacial electron transfer from the conduction band to triiodide ions in the electrolyte (R_{rec}). The logarithm of the R_{rec} values, derived from the impedance data, are plotted in Figure 3b as a function of bias voltage. R_{rec} increases when the temperature is decreased, giving evidence for a higher energetic barrier for recombination of the conduction band electron with triiodide.

The frequency yielding the maximum of the imaginary impedance component of the large hemicircle in the Nyquist plot corresponds to the inverse relaxation time, which can in turn be interpreted as the electron lifetime or "recombination time" as electrons injected from the front contact are lost via capture by

dx.doi.org/10.1021/ja110541t |J. Am. Chem. Soc. XXXX, XXX, 000–000

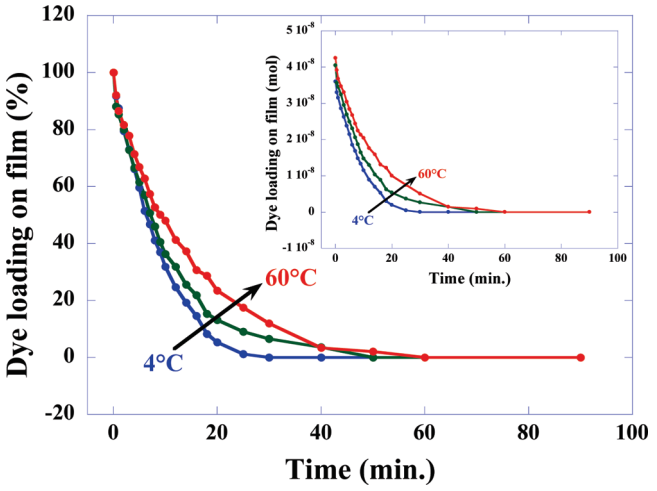

Figure 5. Kinetic of dye desorption as a function of temperature of sensitization (normalized by the total amount of dye). In the inset is shown this same evolution without the dye amount being normalized.

triiodide ions in the electrolyte formed by hole injection at the back contact of the cell.[22] The logarithm of the electron lifetime is also included in Figure 3b as a function of the bias voltage. It is a remarkable observation that by decreasing the grafting temperature of the sensitizer, the electron lifetime increases several times. This finding is consistent with the higher resistance of recombination, explaining the evolution toward higher cell V_{oc} values. This explanation is further supported by the fact that the cell capacitance seems to not be a function of the temperature of sensitization (Figure S1 of the Supporting Information).

ATR-FTIR spectroscopy was applied to gain further insight into the effect of the dye grafting temperature on the cell efficiency. At first sight, the spectra reported in Figure 4 show very similar features and indicate that the mode of grafting is bidentate via the two carboxylate units regardless of the temperature utilized (absence of C═O elongation band of the carboxylic acid group nearby 1720 cm^{-1}). These results also suggest that the modification of the adsorption temperature does not lead to additional poorly grafted dye units maintaining the carboxylic acid function. It also shows that the DINHOP used in conjunction with the C101 dye to prevent its aggregation is truly

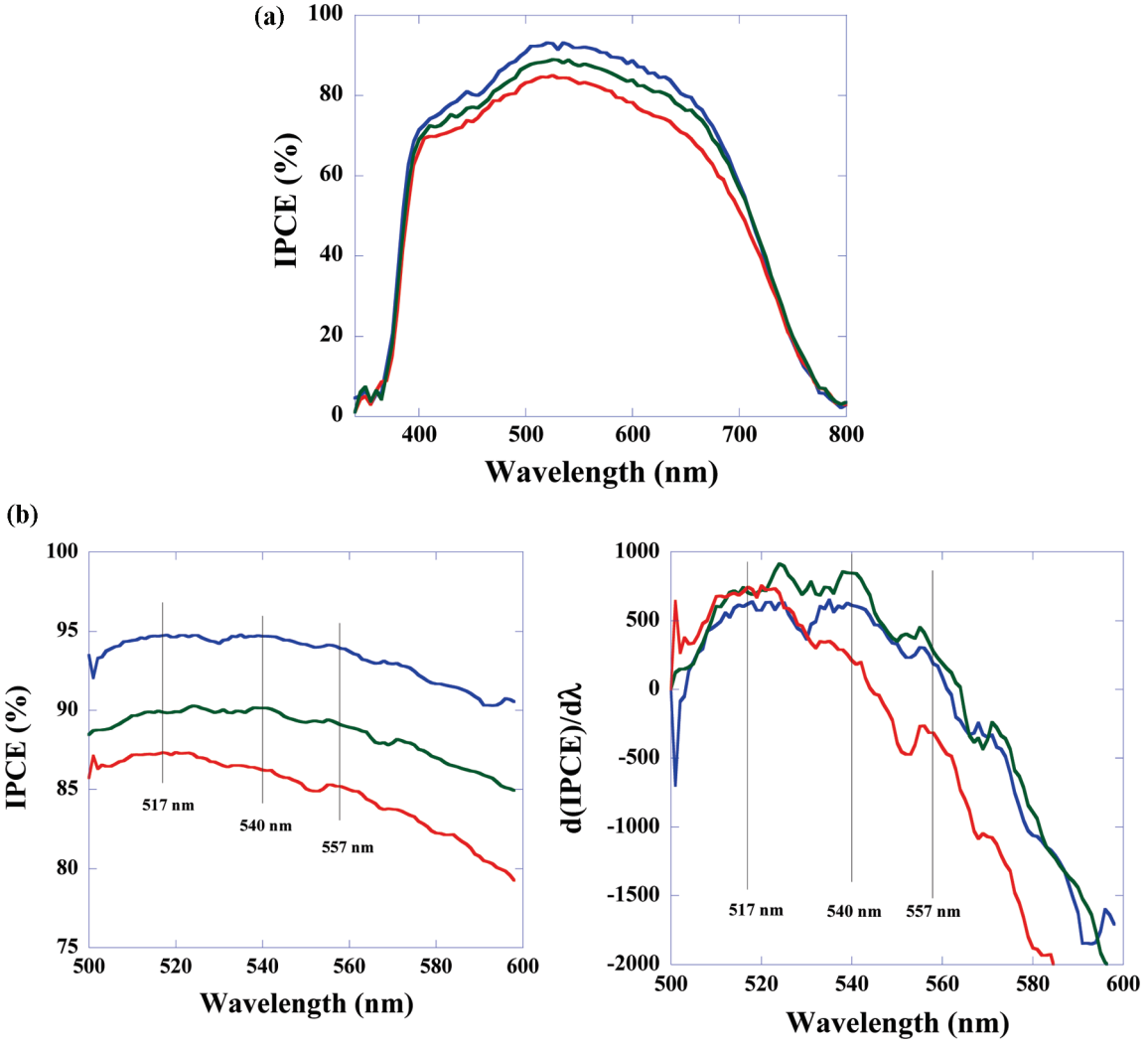

Figure 6. (a) IPCE spectrum as a function of temperature of sensitization and (b) IPCE spectrum scanned each 1 nm between 500 and 600 nm wavelengths with its derivative curve.

dx.doi.org/10.1021/ja110541t |J. Am. Chem. Soc. XXXX, XXX, 000–000

coadsorbed onto the TiO_2 surface on the basis of the increase of the $\nu(CH_3)/\nu(CH_2)$ intensity ratio compared to the film containing only the C101 (Figure S2 of the Supporting Information).

Nevertheless, close comparison of FTIR spectra recorded reveals small changes in the absorption bands as a result of the change in the temperature of dye adsorption (all positions gathered in Table S3 in the Supporting Information). For instance, after deconvolution and fitting of the band profile, the C−H stretching bands from the C_6H_{13} aliphatic chain or the peaks from the NCS group shift by up to 2 cm^{-1}. Likewise, the ratio of the intensity for the $\nu(COO^-)_{sym}$ band and the superimposed contribution for ν(bpy) and $\nu(COO^-)_{asym}$ at 1608 cm^{-1} increases from 0.82 to 0.97 upon decreasing the temperature while the asymmetric mode of $\nu(COO^-)$ together with bpy stretching remains surprisingly unchanged (Figure 4). These results indicate a modification of the dye structure/geometry or dye-to-dye interactions on the TiO_2 surface induced by the adsorption temperature.

The rate of dye desorption was found to decrease with the adsorption temperature, kinetic data being shown in Figure 5. The slow down occurs predominantly during the final phase of the desorption process when the dye loading has decreased below 50%. For films sensitized at 4 °C the total amount of dye desorbed is close to the amount expected for a complete monolayer assuming an area of 1.74 nm^2/(adsorbed molecule), i.e., 3.6×10^{-8} mol, while the dye coverage exceeds the monolayer saturation limit by 12 and 18% at 20 and 60 °C, respectively (S_{film} = 0.283 cm^2 using 8.5 μm + 6.5 μm DSL 18NR-AO double layer photoanode's configuration) indicating formation of multilayer or dye aggregates. Trapping of the latter species in the mesoporous titania film is likely to account for the delay in the desorption at higher temperatures observed in Figure 5.

IPCE spectra measured with films prepared at the three adsorption temperatures are presented in Figure 6a. In keeping with the J_{sc} measurements presented in Figure 2 and Tables 1, S1, and S2, the IPCE values across the visible range increase with decreasing dye absorption temperature, the highest values being obtained with the films loaded at 4 °C. Its integration over the AM 1.5 solar emission gives J_{sc} =19.4 mA/cm^2. The discrepancy of 4% with respect to the current density recorded on our solar simulator is ascribed to a solar spectrum mismatch. Interestingly, looking carefully at the IPCE spectrum in the 500−600 nm wavelength range and its derivative as a function of the wavelength, we can distinguish diverse features for instance at 517, 540, or 557 nm that contribute with a different proportion on the entire spectrum (Figure 6b). The conversion becomes more particularly pronounced toward the red region for films sensitized at 4 °C. This important step forward is the result of the greater electron lifetime that allows collecting more efficiently the electrons generated contrary to the TCO side (originating mainly from the conversion of red photons). The combination between lower dye loading and higher IPCE also indicates that the APCE(λ), given by the product $\eta_{inj}(\lambda)\,\eta_{col}(\lambda)\,\eta_{reg}(\lambda)$, gets improved in a noticeable way. In addition, on the basis of our experimental observations, we could also speculate on stacking of the thiophene unit of the ancillary ligand that affords a more efficient π orbitals overlap when lowering the temperature.

All of these results support the notion that dye adsorption temperature influences (i) the structural characteristics of the self-assembled monolayer and (ii) the importance of the geometry on the electron transfer dynamics and light harvesting properties of the film.

CONCLUSIONS

A significant effect of dye adsorption temperature on the dye-sensitized solar cell using C101-sensitized nanocrystalline titania films has been witnessed. Impedance analysis reveals that the recombination resistance is increased upon lowering the grafting temperature from 60 to 4 °C. The effect is probably caused by an increase in structural order of the self-assembled dye layer upon lowering the adsorption temperature, which appears to be maintained at ambient temperature at least over 1 week. This beneficial aspect demonstrated in this work has also been experienced with the closely related hydrophobic Z907Na dye (Table S4 of the Supporting Information). However, exploring this effect for other widely used ruthenium dye is limited by the drop of dye solubility when reducing its adsorption temperature

ASSOCIATED CONTENT

Supporting Information. Text detailing the experimental part, table listing reproducibility of the PV characteristics recorded with C101 at different temperatures of sensitization, average PV values using sensitized spot electrodes, the main band positions of the C101 dye anchored onto the TiO_2 surface as a function of the temperature of sensitization, and PV characteristics obtained with Z907Na, N719, and N749 dyes, and figures showing the evolution of cell capacitance as a function of photovoltage for cells sensitized at different temperatures and ATR-FTIR spectra of TiO_2 nanocrystalline film sensitized in a solution of 4:1 ratio of C101/DINHOP and C101 alone. This material is available free of charge via the Internet at http://pubs.acs.org

AUTHOR INFORMATION

Corresponding Author

frederic.sauvage@u-picardie.fr; michael.graetzel @epfl.ch

ACKNOWLEDGMENT

F.S., J.-D.D., S.M.Z. P.C., Md.N., and M.G. acknowledge financial support of this work by EU Project "ROBUST DSC", Grant Agreement No. 212792, Dyesol for providing us TiO_2 colloid, and Dr. Robin Humphry-Baker and Dr. Carole Grätzel for fruitful discussion. M.Z. and P.W. thank the National Key Scientific Program (Grant No. 2007CB936700) for financial support.

REFERENCES

(1) O'Regan, B.; Grätzel, M. *Nature* **1991**, *353*, 737.
(2) Chiba, Y.; Islam, A.; Wanatabe, Y.; Komiya, R.; Koide, N.; Han, L. *Jpn. J. Appl. Phys.* **2006**, *45* (25), L638.
(3) Noda, K. *DSC-IC conference*, Colorado Springs, CO, USA, Nov 1−4, 2010.
(4) Frank, A. J.; Kopidakis, N.; Van de Lagemaat, J. *Coord. Chem. Rev.* **2004**, *248*, 1165.
(5) Kay, A.; Grätzel, M. *Chem. Mater.* **2002**, *14*, 2930.
(6) Palomares, E.; Clifford, J. N.; Haque, S. A.; Lutz, T.; Durrant, J. R. *Chem. Commun. (Cambridge, U. K.)* **2002**, 1464.
(7) Menzies, D. B.; Dai, Q.; Bourgeois, L.; Caruso, R. A.; Cheng, Y.-B.; Simon, G. P.; Spiccia, L. *Nanotechnology* **2007**, *18*, 125608.
(8) Grätzel, M. *J. Photochem. Photobiol., A* **2004**, *164*, 3.
(9) Kay, A.; Grätzel, M. *J. Phys. Chem. B* **1993**, *97*, 6272.
(10) Wang, P.; Zakeeruddin, S. M.; Humphry-Baker, R.; Moser, J. E.; Grätzel, M. *Adv. Mater.* **2003**, *15*, 2101.

(11) Wang, P.; Zakeeruddin, S. M.; Humphry-Baker, R; Grätzel, M. *Chem. Mater.* **2004**, *16*, 2694.
(12) Koo, H.-J.; Yoo, P. B.; Yoo, K.; Kim, K.; Park, N.-G. *Inorg. Chim. Acta* **2008**, *361*, 677.
(13) Mihi, A.; Miguez, H. *J. Phys. Chem. B* **2005**, *109*, 15968.
(14) Mihi, A.; Lopez-Alcaraz, F. J.; Miguez, H. *Appl. Phys. Lett.* **2006**, *88*, 193110.
(15) Chen, C. Y.; Wu, S. J.; Wu, C. G.; Chen, J. G.; Ho, K. C. *Angew. Chem.* **2006**, *118*, 5954.
(16) Chen, C. Y.; Wu, S. J.; Li, J. Y.; Wu, C. G.; Chen, J. G.; Ho, K. C. *Adv. Mater.* **2007**, *19*, 3888.
(17) Chen, C. Y.; Wang, M.; Li, J. Y.; Pootrakulchote, N.; Alibabaci, L.; Ngoc-Le, C.; Decoppet, J. D.; Tsai, J. H.; Grätzel, C.; Wu, C. G.; Zakeeruddin, S. M.; Grätzel, M. *ACS Nano* **2009**, *10*, 3103.
(18) Gao, F.; Wang, Y.; Shi, D.; Zhang, J.; Wang, M.; Jing, X.; Humphry-Baker, R.; Wang, P.; Zakeeruddin, S. M.; Grätzel, M. *J. Am. Chem. Soc.* **2008**, *130*, 10720.
(19) Cao, Y.; Bai, Y.; Yu, Q.; Cheng, Y.; Liu, S.; Shi, D.; Gao, F.; Wang, P. *J. Phys. Chem. C* **2009**, *113*, 6290.
(20) Gao, F.; Wang, Y.; Zhang, J.; Shi, D.; Wang, M.; Humphry-Baker, R.; Wang, P.; Zakeeruddin, S. M.; Grätzel, M. *Chem. Commun. (Cambridge, U. K.)* **2008**, 2635.
(21) Zakeeruddin, S. M.; Nazeeruddin, M. K.; Humphry-Baker, R.; Péchy, P.; Quagliotto, P.; Barolo, C.; Viscard, G.; Grätzel, M. *Langmuir* **2002**, *18*, 952.
(22) Bisquert, J. *J. Phys. Chem. B* **2002**, *106*, 325.
(23) Kuang, D.; Klein, C.; Zhang, Z.; Ito, S.; Moser, J. E.; Zakeeruddin, S. M.; Grätzel, M. *Small* **2007**, *12*, 2094.
(24) Wang, Q.; Ito, S.; Grätzel, M.; Fabregat-Santiago, F.; Mora-Sero, I.; Bisquert, J.; Bessho, T.; Imai, H. *J. Phys. Chem. B* **2006**, *110*, 25210.
(25) Bando, K. K.; Mitsuzuka, Y.; Sugino, M.; Sugihara, H.; Sayama, K.; Arakawa, H. *Chem. Lett.* **1999**, 853.
(26) Wang, M.; Li, X.; Lin, H.; Pechy, P.; Zakeeruddin, S. M.; Grätzel, M. *Dalton Trans.* **2009**, *45*, 10015–10020.